Application of a coupledsurface timedependent Hartree grid method to excited state optical spectroscopy

Janet R. Waldeck, José CamposMartínez, and Rob D. Coalson

Citation: J. Chem. Phys. **94**, 2773 (1991); doi: 10.1063/1.459854
View online: http://dx.doi.org/10.1063/1.459854
View Table of Contents: http://jcp.aip.org/resource/1/JCPSA6/v94/i4
Published by the AIP Publishing LLC.

Application of a coupled-surface time-dependent Hartree grid method to excited state optical spectroscopy

Janet R. Waldeck, José Campos-Martínez,[a] and Rob D. Coalson[b]
Department of Chemistry, University of Pittsburgh, Pittsburgh, Pennsylvania 15260

(Received 10 September 1990; accepted 30 October 1990)

The dynamics of multidimensional wave packet motion on nonadiabatically coupled electronic potential surfaces is explored by numerically exact time-dependent quantum mechanics and by the time-dependent Hartree grid (TDHG) approximation. Excellent agreement is found between the TDHG and the exact evolution of the wave packet; in particular, the approximation yields accurate total cross sections for electronic absorption, excitation profiles for resonance Raman scattering, and partial cross sections for photofragmentation in a two degree of freedom model of direct dissociation (which is qualitatively related to experimentally observed processes in methyl halides and ICN).

I. INTRODUCTION

There is currently great interest in understanding the dynamics of molecules in excited electronic states. Such phenomena represent "quantum mechanics in action" in a variety of ways, and have direct bearing on important natural and technological processes. Photodissociation events in isolated molecules, for example, involve chemical bond breaking, and so provide glimpses of elementary chemical reactions in progress. The abundance of experimental information about electronic absorption by laser spectroscopic techniques provides considerable impetus to the theoretician. In particular, frequency domain techniques give accurate, though somewhat indirect, information about the molecular dynamics which ensues following photoabsorption,[1] while recent advances in pump–probe technology promise direct snapshots of excited state evolution behavior.[2]

One of the more exotic features frequently encountered in photodissociation spectroscopy is the breakdown of the Born–Oppenheimer (BO) approximation.[3] This happens upon electronic excitation into energy regions occupied by BO potential surfaces associated with more than one electronic excited state of the molecule. These excited BO surfaces are often "mixed" by terms in the molecular Hamiltonian which are neglected at the BO level of treatment, and this mixing alters spectral signatures associated with the ensuing photodissociation dynamics.[4] Computation of the spectroscopically relevant dynamics remains a challenge for all but the simplest model systems. Indeed, 2–3 spatial degrees of freedom are still the state of the art for exact computations, so the need for accurate approximations amenable to application in many-body systems is great.

One class of techniques which has shown promise in *single*-surface wave packet dynamics applications derives from the time-dependent Hartree (TDH) approximation,[5,6] in which the wave packet is factorized into a product of single degree of freedom packets, and each of these packets is represented by a spatial grid (or some other convenient basis set). Upon utilization of a time-dependent variational principle, appealing equations of motion are obtained. Each degree of freedom evolves according to a one-dimensional Schrödinger equation involving a "mean-field" potential, i.e., the full (coupled many-body) potential energy function averaged over the instantaneous probability densities of all the other degrees of freedom. These equations are much easier to integrate than the Schrödinger equation for the fully coupled system. The TDH evolution is, of course, approximate, but has been found to accurately describe a number of rapid (subpicosecond) processes involving the dynamics of coupled multidimensional systems.[6,7]

A generalization of the TDH equations of motion to problems involving multidimensional wave packet motion on coupled electronic potential surfaces was given recently by Kotler, Nitzan, and Kosloff[8] (KNK), and in a related application to multidimensional tunneling dynamics by Makri and Miller (MM).[9] Both sets of workers were interested in a relatively coarse measure of the underlying quantum dynamics, namely, in nonadiabatic transition language, the net probability to be on one excited Born–Oppenheimer surface or the other. We wished to see if the multisurface TDH grid (TDHG) method was accurate enough to describe the detailed state of the nuclear degrees of freedom on each of these electronic surfaces, as probed by frequency domain electronic spectroscopy. In particular we have utilized this method to compute total cross sections for electronic absorption, excitation profiles for resonance Raman scattering, and partial cross sections for photofragmentation in a two degree of freedom model of direct dissociation (which is qualitatively related to experimentally observed processes in methyl halides[1(a)] and ICN[1(b)]). The results we have obtained are, in general, quite good; the purpose of this paper is to communicate some of our findings.

In Sec. II we describe the excited state spectroscopy of interest to us. Theoretical modeling of these processes requires knowledge of multisurface wave packet evolution, which leads naturally to consideration of multisurface Har-

[a] Fullbright Fellow, 1989–1991.
[b] NSF Presidential Young Investigator, Alfred P. Sloan Foundation Fellow, Camille and Henry Dreyfus Teacher–Scholar.

 0021-9606/91/042773-08$03.00

tree grid methodology. In Sec. III we discuss the appropriate equations of motion. In particular, for some applications (e.g., computation of Raman excitation profiles) we need the complete wave function on each surface, including its *overall phase*, and this has required an extension of the KNK/MM equations of motion to allow straightforward, variationally optimized evaluation of this quantity. In Sec. IV we present numerical results which summarize our experience with the two-surface Hartree grid method, and in Sec. V we sketch some ideas for further research in this area.

II. EXCITED STATE SPECTROSCOPY

We consider a system consisting of two degrees of freedom which move on two diabatic potential surfaces V_1 and V_2 coupled by a nonadiabatic coupling function g. The Hamiltonian which governs this motion is[10]

$$\hat{H}_e = |e_1\rangle\langle e_1|H_1 + |e_2\rangle\langle e_2|H_2 + (|e_1\rangle\langle e_2| + |e_2\rangle\langle e_1|)g, \tag{2.1}$$

where $|e_{1,2}\rangle$ are (structureless) diabatic electronic states, and $H_{1,2} = T + V_{1,2}$ are the nuclear coordinate Hamiltonians for motion on isolated diabatic surfaces $V_{1,2}$, respectively. (T is, of course, the relevant kinetic energy operator.) If a molecule is excited by visible or uv light from a third, ground state potential surface into resonance with the surfaces $V_{1,2}$, then absorption into the excited states, Raman scattering of light through them, and photodissociation of the molecule on them, can take place. The details of the frequency spectra associated with these events follow from the evolution of a particular two-component nuclear wave packet according to the Hamiltonian (2.1). We consider here the commonly encountered case that only one of the zeroth order excited surfaces, say $|e_1\rangle$, is radiatively coupled to the ground electronic state, and furthermore, that the nuclear coordinate dependence of the radiative dipole operator is weak (the Condon approximation[4(b)]). Then the essential wave packet evolution needed to extract frequency spectra is the vibrational eigenfunction $\varphi_g^{(0)}(x,y)$ of the electronic ground state manifold, "placed" on surface V_1 at $t=0$ and propagated subsequently according to the coupled surface Hamiltonian (2.1). (As the superscript on $\varphi_g^{(0)}$ indicates, we consider for notational simplicity the case that the molecule is prepared in its vibrational ground state in the electronic ground state prior to optical excitation; systems with initially excited vibrational motion can be treated analogously.) To express this mathematically, we write a general two-component excited state wave packet as

$$|\Psi(t)\rangle = \varphi_1(x,y,t)|e_1\rangle + \varphi_2(x,y,t)|e_2\rangle. \tag{2.2}$$

Starting from the initial state $|\Psi_0\rangle = \varphi_g^{(0)}(x,y)|e_1\rangle$, we propagate $|\Psi(t)\rangle$ according to $i\partial_t|\Psi(t)\rangle = \hat{H}_e|\Psi(t)\rangle$ (in which we have set $\hbar = 1$). The total absorption cross section at laser frequency ω_L is then given by[4(a),10(a),10(b)]

$$\sigma(\omega_L) = \frac{\mathrm{Re}}{\pi}\int_0^\infty dt \exp[i(\omega_L + E_g^{(0)})t] \times \langle \varphi_g^{(0)}(x,y)|\varphi_1(x,y,t)\rangle. \tag{2.3}$$

where $E_g^{(0)}$ is the vibrational energy eigenvalue corresponding to $\varphi_g^{(0)}$. The Raman cross section to scatter into the final vibrational state $\varphi_g^{(f)}$ on the ground electronic state surface is obtained as $I_{f,0}(\omega_L) = |A_{f,0}(\omega_L)|^2$, with the scattering amplitude $A_{f,0}$ given by[10(a),10(b)]

$$A_{f,0}(\omega_L) = \int_0^\infty dt \exp[i(\omega_L + E_g^{(0)})t] \times \langle \varphi_g^{(f)}(x,y)|\varphi_1(x,y,t)\rangle. \tag{2.4}$$

Finally, if the y coordinate of the system is dissociative, the partial cross section for dissociation into the vth internal state of the vibrational coordinate x on the electronic state $|e_1\rangle$ can be extracted from the overlap,

$$\sigma_1^{(v)}(\omega_L) = |\langle k_1^{(v)}(y)|\langle \chi_1^{(v)}(x)|\varphi_1(x,y,t\to\infty)\rangle|^2, \tag{2.5}$$

where $\chi_1^{(v)}$ is the appropriate vibrational eigenfunction on surface V_1, and $|k_1^{(v)}\rangle$ is an energy-normalized plane-wave state with wave vector determined by conservation of energy.[10(c)] Cross sections for dissociation into electronic state $|e_2\rangle$ can be extracted in the same manner from the asymptotic wave packet $\varphi_2(x,y,t\to\infty)$.

III. THE TWO-SURFACE TIME-DEPENDENT HARTREE GRID METHOD (INCLUDING ALL PHASE INFORMATION)

In order to obtain an approximation to the two-surface wave packet state $|\Psi(t)\rangle$ which is both accurate and applicable to systems with more than 2–3 degrees of freedom, we consider the Hartree trial state

$$|\Psi_T(t)\rangle = \exp\{iS_1\}X_1(x,t)Y_1(y,t)|e_1\rangle + \exp\{iS_2\}X_2(x,t)Y_2(y,t)|e_2\rangle, \tag{3.1}$$

where $X_{1,2}$, $Y_{1,2}$ are single degree of freedom wave packets and $S_{1,2}(t)$ are parameters with temporal but no position dependence. Explicit isolation of the phase/normalization parameter $S_{1,2}$ is inspired by the original single-surface analysis of McLachlan.[5] In the single-surface case this parameterization of the trial wave packet results in simple, one-dimensional mean field-type Schrödinger equations for the spatial packets and an explicit prescription for evaluating the overall wave packet phase. A similar development occurs in the two-surface case.

We subject the trial function (3.1) to Frenkel's variational principle,[11] $0 = \langle \delta\Psi_T|(i\partial_t - \hat{H}_e)|\Psi_T\rangle$. (Although there are several different variational principles, all reduce to Frenkel's version when the trial function is an analytic function of complex variational parameters,[12] as is true here.) By considering arbitrary variations in $|\Psi_T\rangle$ within the constraints imposed by its assumed functional form, optimized equations of motion for the Hartree wave packets and the parameters $S_{1,2}$ can be obtained. To state these in a concise way, it proves convenient to decompose the single-surface zeroth order diabatic potentials into "single degree of freedom" and "interaction" terms, e.g., $V_1(x,y) = u_{1x}(x) + u_{1y}(y) + W_1(x,y)$, and then define single degree of freedom Hamiltonians, e.g., $h_{1x} = T_x + u_{1x}(x)$, T_x being the Cartesian kinetic energy operator associated with coordinate x. With these definitions we obtain the following equations of motion for the Hartree wave packets:

$$i\dot{X}_1 = h_{1x}X_1 + \frac{\langle Y_1|W_1(x,y)|Y_1\rangle}{\langle Y_1|Y_1\rangle}X_1 + \exp\{i[S_2 - S_1]\}\frac{\langle Y_1|g(x,y)|Y_2\rangle}{\langle Y_1|Y_1\rangle}X_2 \quad (3.2a)$$

$$i\dot{X}_2 = h_{2x}X_2 + \frac{\langle Y_2|W_2(x,y)|Y_2\rangle}{\langle Y_2|Y_2\rangle}X_2 + \exp\{i[S_1 - S_2]\}\frac{\langle Y_2|g(x,y)|Y_1\rangle}{\langle Y_2|Y_2\rangle}X_1. \quad (3.2b)$$

The equations of motion for $Y_{1,2}$ are obtained from Eqs. (3.2) by replacing $X \leftrightarrow Y$ and $x \leftrightarrow y$. The phase/norm factor S_1 evolves according to

$$\dot{S}_1 = [\langle Y_1|Y_1\rangle\langle X_1|X_1\rangle^{-1}[\langle Y_1|\langle X_1|W_1(x,y)|X_1\rangle|Y_1\rangle] + \exp\{i[S_2 - S_1]\}\langle Y_1|\langle X_1|g(x,y)|X_2\rangle|Y_2\rangle]. \quad (3.3)$$

$\dot{S}_2$ is analogous with $1 \leftrightarrow 2$. The equations of motion indicated in Eqs. (3.2) and (3.3) bear a strong resemblance to those derived by KNK/MM.[8,9] The main difference is the presence of the (complex) phase/norm parameters $S_{1,2}$ in the present set. Our equations provide a straightforward prescription for updating the system's state function if its current state function is known. Therefore, they give an approximation to the complete nuclear wave packet, e.g., $\exp\{iS_1\}X_1(x,t)\,Y_1(y,t)$ is the amplitude to be at nuclear position (x,y) and in electronic state $|e_1\rangle$. This prediction includes the overall phase of the nuclear wave packet associated with each electronic state, which was omitted in the KNK/MM treatment. For the applications considered by KNK/MM, this phase information was irrelevant. For the computation of Raman spectra, on the other hand, it must be accurately accounted for.

The equations of motion introduced above have one quirk which is well known in Hartree-type coupled-surface wave packet propagation schemes. If the wave packet starts initially on one surface only, say V_1, the evolution equations are ill-defined at $t = 0$ (since either X_2 or Y_2 must be identically zero). This problem can be surmounted by "jump starting" the wave packet on V_2 using the short-time behavior predicted by the full Schrödinger equation.[8(a),13] It is clear that after a short-time interval Δt

$$\varphi_2(x,y,\Delta t) \cong -ig(x,y)X_1(x,0)\,Y_1(y,0)\Delta t. \quad (3.4)$$

Thus, for nonadiabatic coupling functions g that factor into $g(x,y) = g_x(x)g_y(y)$, we set $X_2(x,0) = g_x(x)X_1(x,0)$ and $Y_2(y,0) = -ig_y(y)\,Y_1(y,0)\Delta t$, and find that as Δt is reduced all macroscopic-time wave packet dynamics quickly reaches a stable limit.

IV. RESULTS AND DISCUSSION

The wave packet equations of motion presented in the previous section were implemented for a simple Beswick–Jortner[14] (BJ)-type model of molecular photodissociation. This model involves two coupled spatial degrees of freedom, both of which are bound in the electronic ground state, but one of which is dissociative upon electronic excitation. The model as introduced by Beswick and Jortner utilizes a single excited potential surface of the form

$$V_1(x,y) = A_1\exp\{-\alpha_1[y - \gamma_1 x]\} + \tfrac{1}{2}k_1x^2 + V_1^{(0)}, \quad (4.1)$$

which results in direct dissociation along the y coordinate and in the process induces vibrational activity in the x coordinate. This model provides a qualitative representation of the photodissociation dynamics of both CH_3I[1(a)] and ICN.[1(b)] It corresponds to a simple bond breaking mechanism (e.g., via promotion of an electron from a bonding to an antibonding orbital) and couples the dissociative motion to an anharmonic vibration. For our calculations we use *two* BJ-type surfaces, one for V_1 and one for V_2, with parameters chosen such that V_1 and V_2 cross near the region where the initial wave packet is prepared on surface 1.

It is less obvious what characteristics the nonadiabatic coupling function should possess. These details constitute an outstanding problem in electronic structure theory,[4(a),15] but the usual assumption invoked in simple dynamical theories (such as the Landau–Zener approximation[16]) is that the strength of the nonadiabatic coupling function in the crossing region is the salient feature. This will be the case if the coupling function does not vary too rapidly in the relevant region of nuclear coordinate space. It is also necessary to assume that the nonadiabatic coupling decays to zero as the molecule falls apart in order to trap the fragments on one diabatic surface or the other, as is usually observed experimentally.[1] Consistent with these assumptions is a localized coupling function, e.g., $g(x,y) = g_0\exp\{-\alpha(y - y_0)^2\}$, where $\alpha^{-1/2}$ is roughly the distance from the crossing point y_0 at which the nonadiabatic coupling "turns off," and g_0 is the coupling strength at the crossing. We find that the wave packet dynamics and corresponding frequency spectra are particularly simple in this case. We have also investigated the case where the nonadiabatic coupling is *not* localized in the crossing region, but instead becomes very large inside the crossing region. This is represented by the exponential form $g(x,y) = g_0\exp\{-\alpha(y - y_0)\}$. The value of the coupling at the crossing is still g_0, but the function grows rapidly inside the crossing (depending on the value of α^{-1} which sets the length scale of the exponential function). The spectra associated with exponentially growing nonadiabatic coupling functions can be more elaborate than in the case of localized coupling. This is a reflection of the more complicated wave packet dynamics which arises from the more extended nonadiabatic coupling between diabatic potential surfaces.

In Table I are listed the parameters used in the set of calculations to be presented next. We begin with the localized coupling case. Cuts of the appropriate diabatic surfaces and nonadiabatic coupling functions through the asymptotic equilibrium point $x = 0$ are shown in Fig. 1(a). The value of g_0 was chosen to generate 50% transmission to the dark surface, i.e., the integrated probability is 0.5 on each surface (or, equivalently, the areas under the summed bright vs dark potential cross sections are the same). Two-dimensional contour plots of the initial wave packet (as well as subsequent wave packet dynamics to be discussed below) are shown in Fig. 2. This wave packet is of the form $\varphi_1(x,y,0) = N\exp\{-A_x(x - x_s)^2\}\exp\{-A_y(y - y_s)^2\}$, where N

TABLE I. Parameters used to generate the potential energy surfaces V_1 and V_2, and the coupling function g. $V_n(x,y) = A_n \exp\{-\alpha_n[y-\gamma_n x]\} + \frac{1}{2}k_n x^2 + V_n^{(0)}$, while $g(x,y) = g_0 \exp\{-\alpha(y-y_0)^2\}$ (localized case) and $g(x,y) = g_0 \exp\{-\alpha(y-y_0)\}$ (nonlocalized case). The starting position for the wave packet along the dissociative coordinate is given by y_s.

Potential parameters ($n = 1,2$)					
	A_n	α_n	γ_n	k_n	$V_n^{(0)}$
(1)	13.71	0.4547	0.9850	43.28	4.0
(2)	34.04	0.4547	0.9850	43.28	0.0
Coupling parameters (resulting in 50% transmission)					
		g_0	α	y_0	y_s
Localized)		0.80	0.668	3.5	2.5
Nonlocalized)		5.7	0.668	0.0	2.5
		10.5	0.668	0.0	1.25

is a normalization constant, $A_{x,y}$ prescribe the spread of the wave packet in the x,y directions, respectively, and x_s,y_s specify the location of the center of each Gaussian factor. In the calculations presented below we choose $A_x = 3.29$, $A_y = 0.754$, and $x_s = 0.665$ throughout. The parameter y_s which sets the starting location of the wave packet in the y coordinate is varied to explore various aspects of nonadiabatic coupling. Factorization of the initial wave packet in this manner is necessary to assure asymptotic stability of the wave packets which emerge on both surfaces after the dissociation. Formally this constitutes a weakness of the TDHG method as applied to photodissociation dynamics, but in practice the neglected correlation in $\varphi_g^{(0)}(x,y)$ is often small, due to disparities in the force constants appropriate to the vibrational motion in the ground electronic state.[7]

We focus now on the dynamics of the dissociating wave packet. A glance at the partial cross sections for dissociation

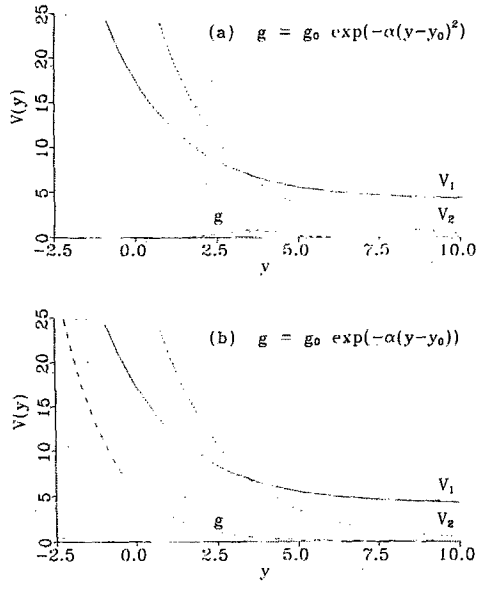

FIG. 1. One-dimensional cut of the diabatic potential surfaces, V_1 (solid) and V_2 (dotted line), through the asymptotic equilibrium point $x = 0$. The dashed line depicts the localized (a) and nonlocalized (b) nonradiative coupling functions $g(x,y)$ via which these potentials interact.

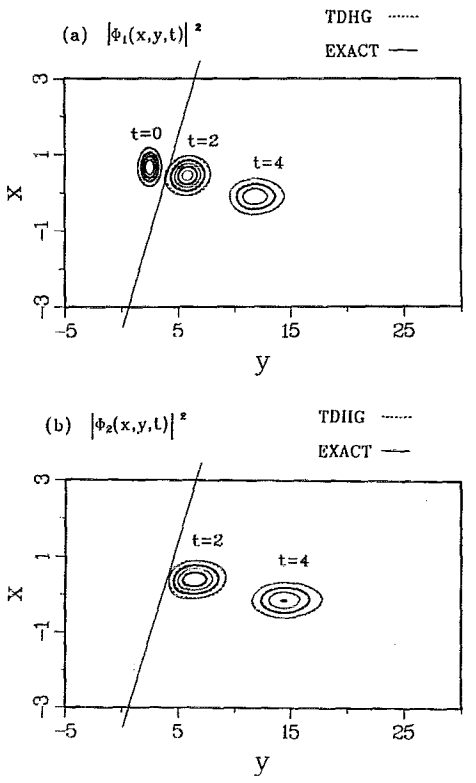

FIG. 2. Exact (solid) and TDHG (dashed line) probability densities for times = 0.0, 2.0, 4.0 on the (a)bright surface V_1 and (b) dark surface V_2, for localized coupling g. The abscissa and ordinate are the dissociative and bound coordinates, respectively. The straight line denotes the V_1–V_2 crossing seam. The starting position for the initial wave packet along the dissociative coordinate $y_s = 2.5$.

onto the dark surface presented in Fig. 3, shows that the two-surface TDHG approximation is excellent for this problem. Recall that partial cross sections probe motion over the entire dissociation trajectory, and, since they involve overlap of the outgoing wave packets with asymptotic eigenfunctions of the diabatic potential energy surfaces, are intricately dependent on the details of the exiting wave packets. The fact that the dark surface partial cross sections are so well reproduced by the two-dimensional TDHG approximation in a case of *strong* nonadiabatic coupling (50% transmission) is encouraging. It also bodes well for the accuracy of shorter

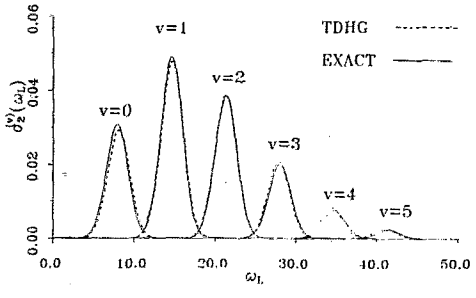

FIG. 3. Exact (solid) and TDHG (dashed line) partial cross sections for population of the asymptotic vibrational eigenstates ($v = 0$–5) on the dark potential energy surface V_2, for localized coupling and 50% transmission to the dark surface.

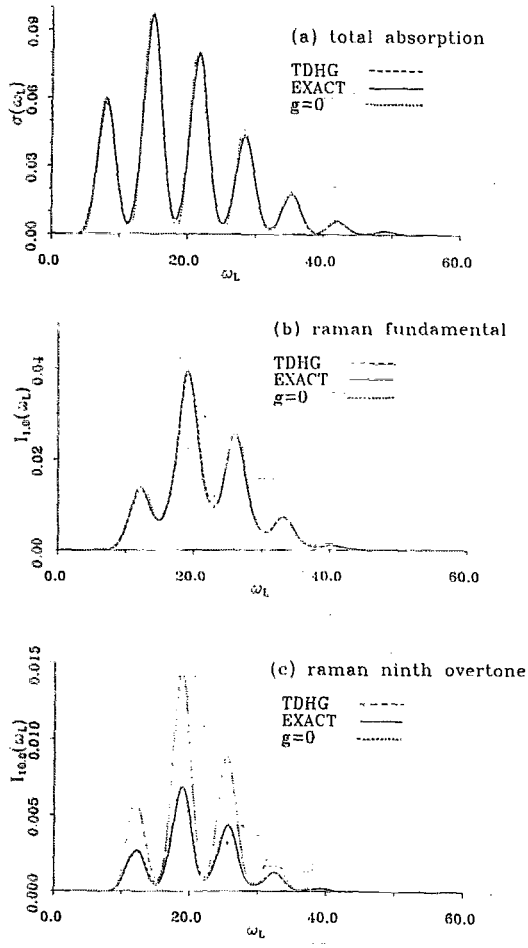

FIG. 4. Exact (solid) and TDHG (dashed line) representing: (a) total absorption cross section, (b) Raman fundamental ($f=1$), and (c) Raman ninth overtone ($f=10$), in the case of localized coupling and 50% transmission to the dark surface. In each panel, a dotted line denotes the results obtained when running the wave packet only on V_1 (i.e., 0% transmission to the dark surface).

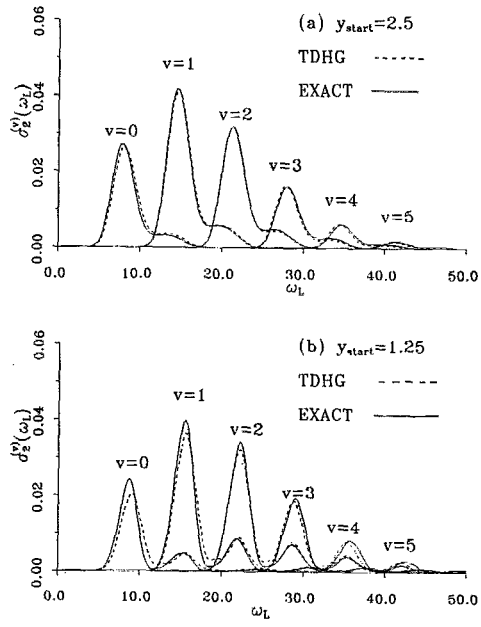

FIG. 5. Dark surface partials cross sections, as in Fig. 3, but for nonlocalized coupling function g, (a) $y_s = 2.5$ and (b) $y_s = 1.25$. Note how these cross sections become more complicated as y_s is moved further inside the crossing region.

time dynamics associated with the same model parameters.

That is indeed the case, as shown by looking at Raman excitation profiles in Fig. 4 corresponding to ground state vibrational transitions in the dissociative mode y. Successively higher electronic Raman overtones are sensitive to the dynamics of the initial wave packet on the excited potential energy surface at successively longer times.[17] Consistent with this behavior we see, in Fig. 4(a), that the total absorption cross section (which is equivalent to, but experimentally more accessible than, the elastic or Rayleigh scattering cross section) is essentially unperturbed by nonadiabatic coupling effects. However, the Raman fundamental is clearly suppressed by the nonadiabatic coupling, and this effect becomes more pronounced for higher overtones.

All of these frequency domain results are qualitatively explained by the wave packet dynamics illustrated in Fig. 2. The most important feature derives from the localized nature of $g(x,y)$. Namely, the wave packet remains entirely on the bright surface until it passes through the crossing seam, at which point a piece is "shaved off," i.e., created on the dark surface. As the bright and dark surface wave packets pass beyond the crossing region, they are quickly trapped on their respective surfaces. Keeping this dynamics in mind, it is easy to see how the lower-order Raman overtones may be only weakly perturbed by the nonadiabatic coupling [depending on where the Franck–Condon (FC) region is relative to the crossing seam]. On the other hand, higher-order Raman overtones, whose time kernels are large at times on the order of or later than the crossing time will be strongly perturbed by strong nonadiabatic coupling. Furthermore, the dominant nonadiabatic effect upon the Raman excitation profiles is "suppression," since part of the wave packet leaks to the dark surface, and the Raman time kernel $\langle \varphi_g^{(f)}(x,y)|\varphi_1(x,y,t)\rangle$ is correspondingly reduced.[10(a),10(b)] Finally, the appearance of fragments on the radiatively dark surface is a direct manifestation of nonadiabatic coupling. The fact that simple, Gaussianesque line shapes are obtained reflects the simple, nearly Gaussian shape of the wave packet (or more directly, the corresponding momentum distribution) which is created on the dark surface in the case of localized nonadiabatic coupling.

It is interesting to compare the results just presented to analogous results obtained when the nonadiabatic coupling function is highly nonlocal. In particular, we utilized an exponential coupling function characterized by $\alpha = 0.668$, $y_0 = 0.0$, and $g_0 = 5.7$. With these parameters we again obtained 50% transmission, but the details of the various cross sections are somewhat different than for the localized case. Most noticeable is the more complicated structure of the dark partial cross sections, displayed in Fig. 5(a). Each of these has an extra shoulder on its high frequency side. Less

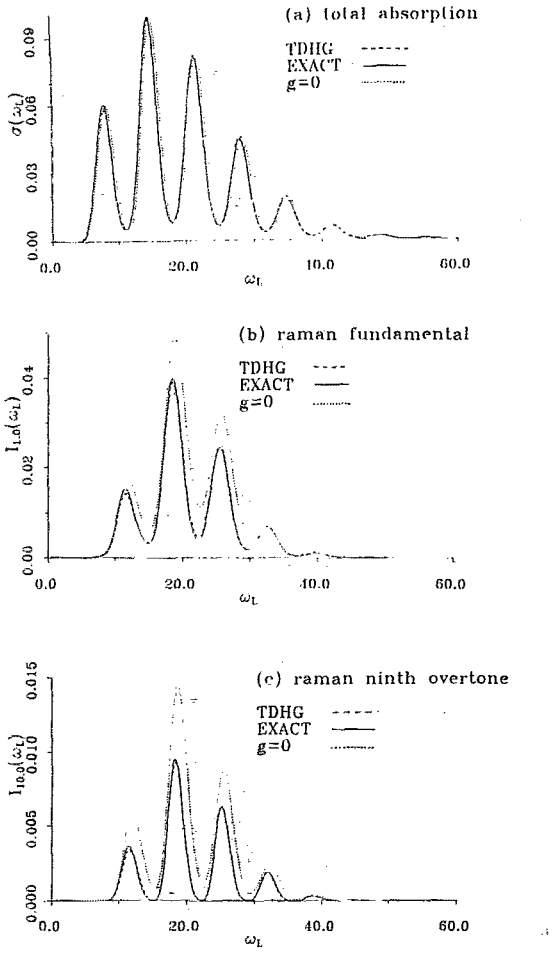

FIG. 6. Absorption spectrum and Raman excitation profiles, as in Fig. 4, but for nonlocalized coupling function and initial conditions associated with Fig. 5(a).

dramatic differences are found for the absorption/Raman excitation profiles, although the presence of strong nonadiabatic coupling inside the crossing region does appear to perturb the Raman profiles slightly more than in the case of localized coupling. [Compare the profiles in Figs. 6(a) and 6(b) to those in Figs. 4(a) and 4(b).] In addition, we noticed that wave packets in the presence of coupling tended to move more slowly along the dissociative coordinate: this could explain the slightly enhanced ninth Raman overtone for the nonlocalized coupling case, which experiences coupling further inside the crossing seam than in the localized case [cf. Figs. 6(c) and 4(c)].

To understand this frequency domain behavior, it is instructive to look at the associated wave packet dynamics depicted in Fig. 7. Because the nonadiabatic coupling is so large inside the crossing region, the initial wave packet undergoes some leakage immediately, even though there is a sizable energy gap separating bright and dark surfaces in the FC region. Thus, the wave packet on the dark surface comes to consist approximately of two pieces, one of which is created at early times by the strong nonadiabatic coupling between the two energetically disparate zeroth order surfaces and a second component which is generated when the bright surface wave packet passes through the crossing re-

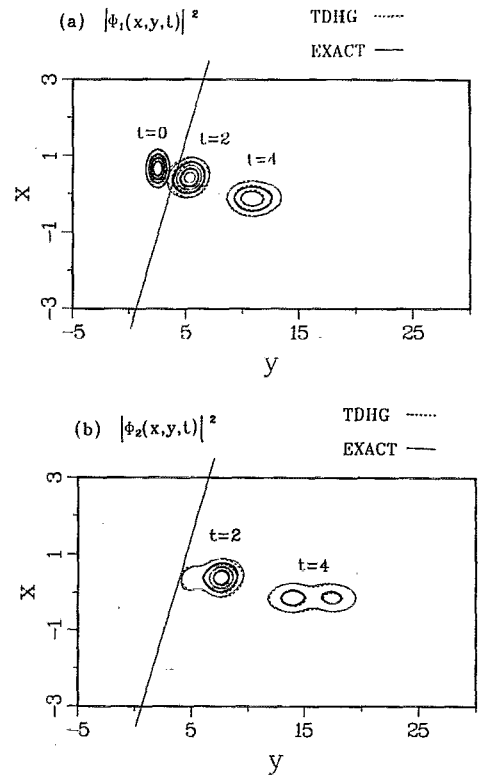

FIG. 7. Probability densities, as in Fig. 2, but for the nonlocalized coupling function g and $y_s = 2.5$. Note that the large value of g inside the crossing region causes some population to leak immediately between surfaces, resulting in a bimodal structure for the wave packet by the time it reaches the crossing seam.

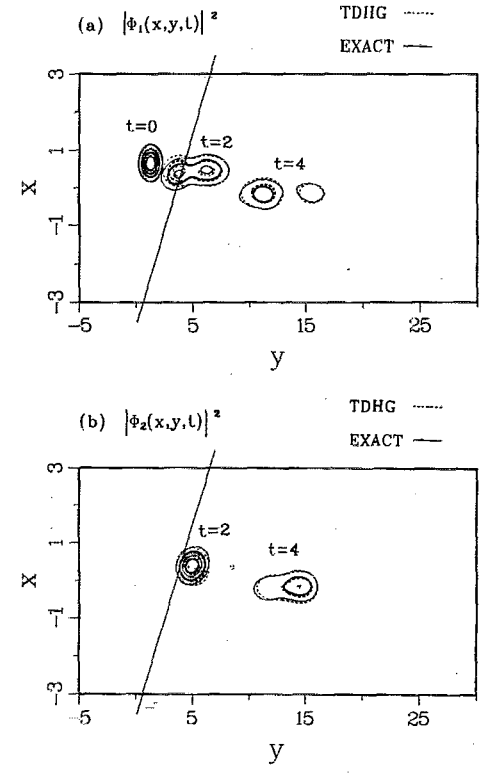

FIG. 8. Probability densities, as in Fig. 7, but now the initial wave packet is moved further inside the crossing, to the starting position $y_s = 1.25$.

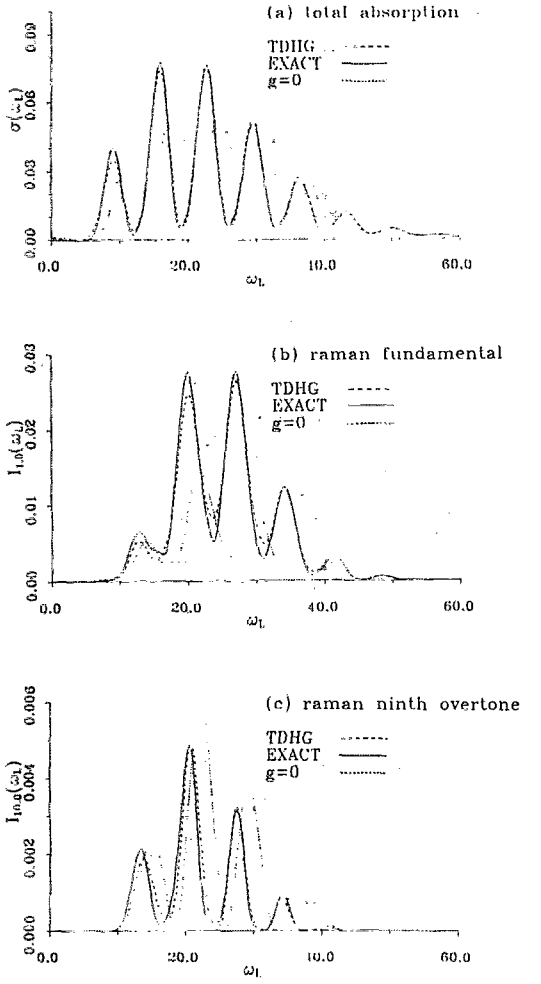

FIG. 9. Absorption spectrum and Raman excitation profiles, as in Fig. 6, but for the case where the initial wave packet is moved further inside the crossing to the starting position $y_s = 1.25$.

gion. This noticeably non-Gaussian wave packet, whose momentum distribution is bimodal, gives rise to the bimodal partial cross sections displayed in Fig. 5(a). Furthermore, the wave packet picture in Fig. 7 illustrates the surprising success of the two-surface TDHG approximation. The two-surface TDHG wave packet dynamics is still quite accurate, even though it is much more intricate than the simple surface-hopping scenario appropriate when the nonadiabatic coupling is localized.

The nonlocalized coupling case implies strong interaction between the wave packets on the two diabatic surfaces from the initial release of the wave packet on the bright surface until a time when both wave packets have passed completely through the crossing. Thus it becomes more difficult to accurately propagate such wave packets as the FC region moves further inside the crossing seam. This behavior is in fact observed. Figure 8 shows the wave packet dynamics on bright and dark surfaces when the initial wave packet is moved further inside the crossing, to the starting position $y_s = 1.25$. We see some erosion in the quantitative accuracy of the TDHG method for evolution on the dark surface at long times. The dark surface partial cross sections are thus expected to be less accurate than in the previous examples. Nevertheless, as seen in Fig. 5(b), they remain quite good, despite the increased complexity relative to those depicted in Fig. 5(a). Furthermore, from Fig. 9 it is seen that the bright surface wave packet also remains accurate for times long enough to extract reliable Raman cross sections over a very wide variety of conditions, even though these spectra are strongly perturbed by the intense early-time coupling between diabatic surfaces 1 and 2.

V. CONCLUSION

In the Hartree approximation the overall system wave packet is forced to factorize into a product of single degree of freedom wave packets. A time-dependent variational principle[5,11] then prescribes "optimal" evolution of each single degree of freedom wave packet. The TDHG trial function is simple to use, yet flexible enough to properly represent many systems of interest. The accuracy of this approximation scheme has been demonstrated in a variety of previous applications.[6–9]

We applied the TDHG formalism to a simple Beswick–Jortner-type two degree of freedom model for molecular dissociation, utilizing two potential energy surfaces which interact nonadiabatically according to a coupling function $g(x,y)$. Very good agreement between the TDHG and the exact evolution of a wave packet was found. In particular, the approximation accurately reproduced the total cross sections for electronic absorption, excitation profiles for resonance Raman scattering and partial cross sections for photofragmentation. The specific function $g(x,y)$ by which the surfaces were coupled played an important role in governing the wave packet dynamics, and thus influenced the resulting spectra. The more extended nonadiabatic coupling between diabatic potential surfaces yielded more complicated wave packet dynamics, and thus more elaborate spectra than seen for the localized coupling case. When the magnitude of $g(x,y)$ was substantial prior to the crossing seam, we found slight degradation in the TDHG results, but overall the performance of the approximation was very good.

The only aspect of the dynamics which is improperly described by the TDHG approximation is the "direct correlation" of the motion in various degrees of freedom, or more precisely, the nonfactorizability of the exact multidimensional wave packet which describes the nuclear motion on each diabatic potential energy surface. This manifests itself geometrically as a twisting of the wave packet away from the x–y axes, as is apparent when comparing the exact (solid) vs TDHG (dashed line) wave packets on V_1 and V_2 in Fig. 8. Recently, the TDHG method was extended to include "configuration interaction" for single surface problems.[18] To correct for the neglect of "direct correlation" in factorized Hartree wave packets, a time-dependent superposition of TDHG-type wave packets was constructed. The inclusion of configuration interaction, accomplished via the evolution of the basis coefficients, was shown to significantly improve control over the quality of the results. It is thus natural to contemplate using the TDHG-level approximation studied in the present work as a starting point for construction of a two-surface configuration interaction scheme which can

produce essentially "*ab initio*" wave packet dynamics for multidimensional motion on coupled potential energy surfaces.

ACKNOWLEDGMENTS

The authors are grateful to M. Messina for numerous useful suggestions concerning the computational procedure. This work was supported by a grant from the National Science Foundation, the Petroleum Research Fund, the Alfred P. Sloan Foundation, and the Camille and Henry Dreyfus Foundation. J. C.-M. gratefully acknowledges a grant from the Ministerio de Educacion y Ciencia of Spain and the Fullbright Commission. Many of the computations reported here were performed at the Pittsburgh Supercomputing Center.

[1](a) K. Q. Lao, M. D. Person, P. Xayariboun, and L. J. Butler, J. Chem. Phys. **92**, 823 (1990); (b) J. F. Black, J. R. Waldeck, and R. N. Zare, *ibid.* **92**, 3519 (1990); (c) J. Biesner, L. Schnieder, G. Ahlers, X. Xie, K. H. Welge, M. N. R. Ashfold, and R. N. Dixon, *ibid.* **91**, 2901 (1989).

[2]M. J. Rosker, M. Dantus, and A. H. Zewail, J. Chem. Phys. **89**, 6113 (1988); H. L. Fragnito, J.-Y. Bigot, P. C. Becker, and C. V. Shank, Chem. Phys. Lett. **160**, 101 (1989); R. M. Bowman, M. Dantus, and A. H. Zewail, *ibid.* **156**, 131 (1989); N. F. Scherer, A. J. Ruggiero, M. Du, and G. R. Fleming, J. Chem. Phys. **93**, 856 (1990).

[3]M. Born and J. R. Oppenheimer, Ann. Phys. (Leipzig) **84**, 457 (1927).

[4](a) H. Koppel, W. Domcke, and L. S. Cederbaum, Adv. Chem. Phys. **57**, 59 (1984); (b) G. Stock, R. Schneider, and W. Domcke, J. Chem. Phys. **90**, 7184 (1989); (c) U. Manthe and H. Köppel, J. Chem. Phys. **93**, 345 (1990); **93**, 1658 (1990).

[5]A. D. McLachlan, Mol. Phys. **8**, 39 (1964).

[6]R. H. Bisseling, R. Kosloff, R. B. Gerber, M. A. Ratner, L. Gibson, and C. Cerjan, J. Chem. Phys. **87**, 2760 (1987); R. Alimi and R. B. Gerber, Phys. Rev. Lett. **64**, 1453 (1990); R. Kosloff, J. Phys. Chem. **92**, 2087 (1988).

[7](a) M. Messina and R. D. Coalson, J. Chem. Phys. **90**, 4015 (1989); (b) R. D. Coalson, Chem. Phys. Lett. **165**, 443 (1990); (c) M. Messina and R. D. Coalson, J. Chem. Phys. **92**, 5297 (1990); (d) M. Messina and R. D. Coalson, *ibid.* **92**, 5712 (1990); (e) R. D. Coalson and M. Karplus, *ibid.* **93**, 3919 (1990).

[8]Z. Kotler, A. Nitzan, and R. Kosloff, Chem. Phys. Lett. **153**, 483 (1988).

[9]N. Makri and W. H. Miller, J. Chem. Phys. **87**, 5781 (1987).

[10](a) R. D. Coalson and J. L. Kinsey, J. Chem. Phys. **85**, 4322 (1986); (b) R. D. Coalson, Adv. Chem. Phys. **73**, 605 (1989); (c) J. Chem. Phys. **86**, 6823 (1987).

[11]J. Frenkel, *Wave Mechanics* (Oxford University, Oxford, 1934).

[12]E. J. Heller, J. Chem. Phys. **64**, 63 (1976); J. Kucar, H.-D. Meyer, Chem. Phys. Lett. **140**, 525 (1987).

[13]S.-I. Sawada and H. Metiu, J. Chem. Phys. **84**, 6293 (1986).

[14]J. A. Beswick and J. Jortner, Chem. Phys. **24**, 1 (1977).

[15]F. T. Smith, Phys. Rev. **179**, 111 (1969); R. E. Olson, F. T. Smith, and E. Bauer, Appl. Opt. **10**, 1848 (1971); F. X. Gadea and M. Pelissier, J. Chem. Phys. **93**, 545 (1990).

[16]Compare, L. D. Landau and E. M. Liftshitz, *Quantum Mechanics: Non-Relativistic Theory*, 3rd Ed. (Pergamon, New York, 1977), Chap. XI.

[17]D. Imre, J. L. Kinsey, R. Field, and D. Katatyama, J. Phys. Chem. **86**, 2564 (1982); D. Imre, J. L. Kinsey, A. Sinha, and J. Krenos, *ibid.* **88**, 3956 (1984).

[18]J. Campos-Martinez and R. D. Coalson, J. Chem. Phys. **93**, 4740 (1990).